NASA Technical Memorandum 102271

Analysis of Small-Scale Rotor Hover Performance Data

Cahit Kitaplioglu

March 1990

National Aeronautics and Space Administration

NASA Technical Memorandum 102271

Analysis of Small-Scale Rotor Hover Performance Data

Cahit Kitaplioglu, Ames Research Center, Moffett Field, California

March 1990

National Aeronautics and
Space Administration

Ames Research Center
Moffett Field, California 94035-1000

SUMMARY

Rotor hover-performance data from a 1/6-scale helicopter rotor are analyzed and the data sets compared for the effects of ambient wind, test stand configuration, differing test facilities, and scaling. The data are also compared to full-scale hover data. The data exhibited high scatter, not entirely due to ambient wind conditions. Effects of download on the test stand proved to be the most significant influence on the measured data. Small-scale data correlated reasonably well with full-scale data; the correlation did not improve with Reynolds number corrections.

NOMENCLATURE

c_d	airfoil-section drag coefficient
c_f	skin-friction drag coefficient
c_ℓ	airfoil-section lift coefficient
C_{D0}	rotor drag coefficient
C_P	rotor power coefficient
C_T	rotor thrust coefficient
FM	rotor figure of merit
K	scaling factor
M_{tip}	rotor hover tip Mach number
r, ξ	spanwise variables of integration
R	rotor radius
R_ℓ	flat-plate Reynolds number
Re	Reynolds number
S	equivalent blockage area of test apparatus
V_W	wind speed
α	rotor-blade angle of attack (pitch angle)

σ rotor solidity

Subscripts

c corrected for download effects

fs full scale

ms model scale

1 measured value

INTRODUCTION

Three hover tests of a small-scale helicopter rotor were performed in the facilities of the National Full-Scale Aerodynamic Complex (NFAC). Detailed descriptions of the tests were reported elsewhere (refs. 1 and 2). This report compares the rotor performance data sets obtained during these tests and briefly discusses their differences, which result from the effects of (1) ambient wind, (2) the test stand configuration, (3) the test facility, and (4) scaling.

The three tests, all of which used the same model blades (see table 1 for blade characteristics) and Rotor Test Rig (RTR), were

1. RTR/40 × 80 Test (fig. 1): This hover test of a 1/6-scale, four-bladed Sikorsky S-76 rotor was performed in the test section of the 40- by 80-Foot Wind Tunnel. The rotor was mounted 10 ft above the wind tunnel floor in a thrust down, wake up mode. No foam (for acoustic purposes) was applied to the test rig. The blades did not have any boundary layer tripping devices. The performance data were measured using the RTR internal six-component balance and the torque load cell.

2. RTR/OARF I Test (fig. 2): This hover test of the same 1/6-scale rotor was performed at the Outdoor Aerodynamic Research Facility (OARF). The rotor was mounted 20 ft above the ground in the standard thrust up, wake down mode. A foam cover (to serve as an acoustic anti-reflection treatment) was installed on the external surface of the RTR during part of the test. During two runs, a simple boundary layer tripping device was installed on the blades. Performance data were measured using three vertical load cells installed directly below the RTR, and a torque load cell. Data were obtained over a range of ambient wind conditions.

3. RTR/OARF II Test (fig. 3): For this test, the 1/6-scale rotor was mounted in the same thrust down, wake up mode as in the 40 × 80 test, 10 ft above the ground. The foam covering was in place during the entire test, but no boundary layer tripping device was used. Performance data were measured using three vertical load cells, again installed directly below the RTR, and a torque load cell. Data were obtained over a range of ambient wind conditions.

EFFECT OF AMBIENT WIND

During both OARF I and OARF II tests, data were obtained over a range of ambient wind conditions from 0 m/sec to approximately 3.6 m/sec. A previous full-scale rotor test performed outdoors (ref. 3) indicated that ambient winds of less than 1.3 m/sec have only a small effect on rotary wing performance. Thus, the data were sorted such that those obtained at ambient winds of less than 1.3 m/sec were flagged as low-wind data, and those obtained at greater than or equal to 1.3 m/sec were flagged as high-wind data.

Figures 4 and 5 compare rotor performance data obtained at low- and high-wind conditions during the two tests. For the data in these figures, an acoustic anti-reflection foam cover was in place around the test rig; no boundary layer trip devices were in use. In each figure, second-order polynomials are fitted to the data. These curves indicate a small (<5%) difference between the low-wind and high-wind data; however, in view of the significant data scatter evident in the figures, little influence on rotor performance of ambient wind is indicated when the wind speed is below the maximum 3.6 m/sec encountered. A detailed examination of the data shows that approximately the same amount of data scatter is present at both low and high winds, so it is not clear that the scatter is entirely the result of ambient wind. Data presented in reference 3 demonstrated that data scatter is reduced when a wind-correction procedure is applied; however, for winds less than 3 knots (1.5 m/sec) only a 3% correction in the rotor power coefficient was obtained. (The 40×80 test data, obtained with no ambient wind, also displays scatter; however, this is most likely due to recirculation effects within the enclosed test section.) It should be kept in mind that these performance plots are a measure of the overall behavior of the rotor, not its detailed aerodynamics.

Corresponding aeroacoustic data show significant variations with ambient wind. Figure 6 illustrates the acoustic differences arising from different ambient wind conditions. A prominent feature is the presence of high-amplitude subharmonic spectral components (labeled 1-6 in fig. 6(b)) at the high-wind condition; these are completely absent at low winds. (Note that the "high-wind" condition here is 0.67 m/sec, only half the 1.3 m/sec criterion stated previously.) The subharmonics gradually merge with the blade-passage harmonics as the frequencies increase. The blade passage frequency (BPF) harmonic peak levels are up to 2 dB higher at high ambient winds than at low winds, and there is noticeable frequency broadening. The fact that no significant performance differences were observed between high- and low-wind tests while acoustic spectra differences were clearly present implies that unsteady blade surface-pressure data, rather than mean blade pressures based on overall rotor performance, are required for accurate noise predictions.

EFFECT OF THE TEST STAND CONFIGURATION

The OARF I and II tests were performed with the same rotor at the same facility but in different configurations. In both tests, the rotor thrust was measured with three load cells mounted so as to transmit only vertical forces. The load cells were located between the RTR base and the top of the mounting tower, approximately 2 m below the rotor hub. Check-load calibration during testing demonstrated the high accuracy of the data obtained using this arrangement.

In the OARF I test the rotor had an unobstructed inflow, but the wake impinged on the test hardware located below the rotor. Therefore, during the OARF I test the thrust measurements included download effects. In the OARF II test, the wake was directed to open air, not impinging on the test hardware. Although the flow into the rotor passed over test hardware of significant blockage area, this was assumed to have minimal impact on rotor performance because of the low inflow velocity.

To correct the OARF I data for the download effect, the drag force on the mounting base was estimated (ref. 4, p. 3-16), based on wake velocity calculated from simple momentum theory. The corrected rotor thrust coefficient is given by

$$\left(\frac{C_T}{\sigma}\right)_c = \left(\frac{C_T}{\sigma}\right)\left(1+\frac{S}{\pi R^2}C_{D_0}\right) \tag{1}$$

where S is the blockage area of the mounting base and fairing, and C_{D_0} is the drag coefficient of a rectangular cross-section normal to the flow. The value of the drag coefficient ($C_{D_0} = 1.18$) is approximately constant for the aspect ratio and the range of Reynolds numbers encountered. The rotor power coefficient is assumed to be unaffected and the rotor figure of merit is corrected according to the definition

$$FM = \sqrt{\frac{\sigma}{2}}\,\frac{\left(\frac{C_T}{\sigma}\right)^{3/2}}{\left(\frac{C_P}{\sigma}\right)} \tag{2}$$

Figure 7 compares performance data obtained during the two tests. Both sets of data are for low ambient wind conditions (<1.3 m/sec) with the foam covering in place; boundary layer trips were not in use. Clearly, the download corrections lead to a significant improvement in correlation between the two sets of data. The thrust coefficient at which the peak figure of merit occurs appears to shift slightly between the two tests. Figure 7 illustrates the basic validity of download corrections, and the data in the figure could be used in future tests of similar configurations to make download corrections to data.

EFFECT OF THE FACILITY

Previous tests have indicated that enclosures, even when large compared to rotor size, influence rotor performance. Piziali and Felker (ref. 5) reported the presence of wake re-ingestion during a hover test of a rotor in a chamber having height and cross-section dimensions of 15 and 6 rotor diameters, respectively.

Two tests conducted in this series, the 40 × 80 test and the OARF II test, provided an opportunity to examine this effect. The tests differed from each other in two respects: (1) force measurements during the OARF II test were made with three load cells, whereas the forces during the 40 × 80 test were measured with the RTR internal balance; and (2) the OARF II test was carried out in an open environment

with minimal wake recirculation, whereas the 40 × 80 test was in a closed chamber, albeit large relative to rotor size, which may have led to wake recirculation.

Effect of Different Force Measurement Methods

The RTR internal balance, used to measure the aerodynamic forces on the small-scale rotor during the 40 × 80 hover test, is subject to interactions between its various components. Empirical corrections, based on static calibration data, are normally applied to measured data to account for interaction effects. Static calibration of the balance indicates that torque/thrust interaction is the largest of these effects; it also indicates strong hysteresis behavior under combined-load conditions. A satisfactory explanation of the hysteresis is not presently available. When the rotor is rotating, these interaction and hysteresis effects may change; a dynamic calibration of the internal balance with a rotating load on the rotor head has not been performed to date.

Figure 8 compares the data obtained in the two tests. Two sets of 40 × 80 data are shown: one set with the combined-load interaction corrections, one set without the corrections. Note that these data include enclosure effects, discussed below, as well as differences that may arise from different force measurement methods. It is not immediately clear whether combined-load corrections should be applied to the balance data. The curves indicate that combined-load interaction and hysteresis effects may not be as large under rotating loads as under static loads.

Effect of Test Enclosures

As mentioned before, the two tests were carried out in different environments. In the 40 × 80 test, the wake may have been reingested by the rotor. This was not the case for the OARF II test, where the wake was directed into the open atmosphere with no obstructions.

A hovering rotor experiencing wake reingestion can be considered to be in vertical flight at low speed. Basic helicopter theory (ref. 6) shows that additional rotor power is required for vertical velocity at essentially fixed thrust. Therefore, with wake reingestion one expects lower rotor performance than when wake reingestion is not present; i.e., for the 40 × 80 test, the rotor power curve should be higher and the figure of merit curve should be lower than for the OARF II test. Figure 8 shows that this is the case when the 40 × 80 data are not corrected for combined-load interactions. However, when the 40 × 80 data are corrected for combined-load interactions, the opposite trends are observed.

Shivananda (ref. 7) noted a degradation of rotor performance when testing in a small chamber, in accordance with basic theory, although it should be noted that the test chamber in Shivananda's experiment was not totally closed, there being some small vent holes both above and below the rotor. Piziali and Felker (ref. 5), on the other hand, who tested a small rotor both in a large chamber and outdoors, observed a small improvement (~1.5%) in performance when testing inside the chamber.

Given these uncertainties, the rotor performance data in figure 8 cannot be used to determine if recirculation was present during the 40 × 80 test.

REYNOLDS NUMBER AND SCALING EFFECTS

During the three small-scale tests, the range of blade-tip Mach numbers was typical of full-scale helicopter rotors, so the Reynolds numbers differed by the scale factor of the model blades. The Reynolds numbers, based on blade chord and tip speed, that were encountered during these tests are of the order of 10^6 and are smaller inboard of the tip, thus falling in the critical boundary layer transition region. Full-scale rotors, on the other hand, typically operate at fully turbulent Reynolds numbers of the order of 10^7. Therefore, there is a possibility of laminar separation of the boundary layer on the small-scale blades, particularly at inboard stations.

This can have important effects on both the performance and the acoustics of the rotor. If the laminar boundary layer remains attached, skin-friction drag and rotor power will be lower than for a full-scale rotor. If, on the other hand, there is laminar separation, the large high-pressure separated region could cause a sharp increase in drag and power. Also, laminar vortex shedding is an important source of noise.

Boundary Layer Trips

During the OARF I test, several data runs were made with simple devices installed on the top and bottom surfaces of the rotor blades for the purpose of modifying the boundary layer characteristics. These tripping devices consisted of plain cellophane tape 0.005 cm (0.002 in.) thick with their forward edges located 0.2 blade chords behind the leading edge of the rotor blade.

Because the rotor blades did not contain pressure instrumentation, and flow visualization was not available, there was no way to ascertain either the flow characteristics over the blades or the effect of the trip strips. However, examination of the performance data with and without the trip strips gave a good indication of their effect.

Figure 9 shows a discernible loss of rotor performance (at low-wind conditions) with the addition of the trip strips. When the trip strips were applied, the drag increased, as indicated by the higher rotor power coefficient curve. With reference to the well-known skin-friction drag plots (fig. 10 and ref. 4, p. 2-6), it can be inferred that the boundary layer over the blade was probably not experiencing laminar separation; if it were, tripping the boundary layer would lead to reattachment and an improvement of rotor performance. On the contrary, the addition of the trip strips caused a large enough increase in surface roughness to lead to a jump to the "turbulent" boundary layer curve. This, in turn, led to an increase in the skin-friction drag, which resulted in the measured loss of performance.

In view of these observations, it is hypothesized that without boundary layer trips, these small-scale rotor blades were operating in the laminar (or perhaps transition) but unseparated regime. With the addition of boundary layer trips, the flow jumped to the fully turbulent regime, where full-scale rotors operate, but with an effective skin-friction drag component much larger than that of full-scale rotors.

Comparison with Full-Scale Data

For comparison, data was used from a hover-stand test performed by Sikorsky Aircraft (ref. 8), of a full-scale S-76 rotor similar to that used during this series of small-scale tests. The small-scale tests employed blades with a rectangular tip planform, whereas the Sikorsky test blades had the standard swept-tapered tips, but this difference in planform should have minimal effect in hover since the maximum Mach numbers are lower than transonic. Also note that 3% corrections were applied to the full-scale test data to account for test stand interference and ground effects. Of the three small-scale tests, the OARF I test has the most similarity to the full-scale test; both were performed outdoors in a thrust up, wake down mode with the rotor wake impinging on the test stand.

Differences in Reynolds numbers between the small- and full-scale tests are expected to influence the data significantly. Yamauchi and Johnson (ref. 9) have presented an extensive study of rotor airfoil scaling in which they developed easily implemented scaling laws to account for Reynolds number effects in helicopter airfoil analyses. These can be extended, in a straightforward manner, to rotors (see appendix). The rotor thrust and power coefficients are scaled as follows:

$$\left(\frac{C_T}{\sigma}\right)_{fs} = K\left(\frac{C_T}{\sigma}\right)_{ms} \qquad \left(\frac{C_P}{\sigma}\right)_{fs} = \frac{1}{K}\left(\frac{C_P}{\sigma}\right)_{ms} \tag{3}$$

where

$$K = \left(\frac{Re_{fs}}{Re_{ms}}\right)^{1/5} \tag{4}$$

The rotor figure of merit in hover is defined by equation (2) on page 4. Combining equations (2) and (3) to calculate the rotor figure of merit scaling relation gives

$$FM_{fs} = K^{5/2}\sqrt{\frac{\sigma_{fs}}{\sigma_{ms}}}\, FM_{ms} \tag{5}$$

Figures 11 and 12 show the effect of making these Reynolds number corrections, and figure 13 compares the two OARF data sets corrected for Reynolds number effects with the full-scale data. (The OARF I data were also corrected for download.) No improvement in the correlations among the three data sets is noted with the Reynolds number corrections. Again, the data scatter hinders a more definite conclusion.

CONCLUSIONS

A 1/6-scale helicopter rotor was tested in hover, in a wind tunnel and outdoors, in several different configurations. The influence on rotor performance of the test facility and test configuration were inves-

tigated. The effects of ambient wind and Reynolds number were studied. The following can be concluded:

1. Measured data displayed high scatter that is not entirely due to ambient winds.

2. Ambient winds had only a small effect on rotor performance. However, the data scatter may be masking more significant effects of wind. Acoustic data, more sensitive to rotor unsteadiness, showed definite variation with small changes in ambient wind conditions.

3. Download effects of the wake on the test stand led to about a 15% change in the rotor thrust when the rotor was in the thrust up, wake down configuration.

4. The effect of the test facility could not be clearly discerned because of different force-measurement techniques used during different tests. Also, the RTR balance requires careful calibration under rotating loads.

5. Rudimentary boundary layer tripping increased skin-friction drag and resulted in loss of performance, rather than alleviating laminar separation (if present) to improve performance.

6. Small-scale data, although quite close to full-scale data generally, exhibit significant differences. The correlation did not improve with Reynolds number corrections.

APPENDIX

DERIVATION OF ROTOR REYNOLDS NUMBER SCALING RULES

In general, the rotor thrust can be calculated from the airfoil section lift coefficient, c_ℓ, by integrating along the rotor radius. The resulting rotor thrust coefficient is given by

$$\frac{C_T}{\sigma} = \frac{1}{2R^3} \int_0^R c_\ell(r) \cdot r^2 dr \tag{A1}$$

Similarly, the rotor power coefficient can be obtained from the airfoil drag coefficient, c_d (not considering induced drag, which should not be influenced by Reynolds number):

$$\frac{C_P}{\sigma} = \frac{1}{2R^4} \int_0^R c_d(r) \cdot r^3 dr \tag{A2}$$

The drag and lift coefficients of helicopter rotor airfoil sections are scaled for Reynolds number effects as follows (ref. 9):

$$c_\ell = K c_{\ell_1}\left(\frac{\alpha_1}{K}\right) \tag{A3}$$

$$c_d = \frac{c_{d_\ell}}{K} \tag{A4}$$

where the subscript 1 indicates a measured value and no subscript indicates a scaled value; the measured lift coefficient, c_{ℓ_1}, is a function of a scaled pitch angle given by α_1/K; and the scale factor, K, is defined by $K = (Re/Re_1)^{1/5}$.

In the present study, the measured values were obtained with a small-scale model, and we are interested in calculating the corresponding full-scale values for comparison with measured full-scale data. Accordingly, substituting equation (A3) into equation (A1) and using the geometric scaling transformation

$$r = K^5 \xi \tag{A5}$$

gives the scaling relation for the rotor thrust:

$$\left(\frac{C_T}{\sigma}\right)_{fs} = \frac{1}{2R_{ms}^3} \int_0^{R_{ms}} K c_{\ell_{ms}} \xi^2 d\xi \tag{A6}$$

Using the general definition of thrust coefficient (eq. (A1)) set up for model scale, this becomes

$$\left(\frac{C_T}{\sigma}\right)_{fs} = K\left(\frac{C_T}{\sigma}\right)_{ms} \tag{A7}$$

where the model-scale quantity $(C_T/\sigma)_{ms}$ is evaluated at the scaled pitch angle α_{ms}/K. Similarly, the scaling relation for the rotor power coefficient becomes

$$\left(\frac{C_P}{\sigma}\right)_{fs} = \frac{1}{K}\left(\frac{C_P}{\sigma}\right)_{ms} \tag{A8}$$

REFERENCES

1. Kitaplioglu, C.; and Shinoda, P.: Hover and Forward Flight Acoustics and Performance of a Small-Scale Helicopter Rotor System. 11th European Rotorcraft Forum, Paper 98, London, Sept. 1985.

2. Kitaplioglu, C.: Scaling of Helicopter Main Rotor Noise in Hover. AIAA Paper 86-0393, Jan. 1986.

3. Felker, F. F.; Maisel, M. D.; and Betzina, M. D.: Full-Scale Tilt-Rotor Hover Performance. J. American Helicopter Soc., vol. 31, no. 2, Apr. 1986, pp. 10-18.

4. Hoerner, S. F.: Fluid Dynamic Drag. Published by the author, Bricktown, NJ, 1965.

5. Piziali, R.; and Felker, F: Reduction of Unsteady Circulation in Hovering Model Helicopter Rotor Testing. J. American Helicopter Soc., vol. 32, no. 1, Jan. 1987, pp. 54-59.

6. Gessow, A.; and Myers, G. C., Jr.: Aerodynamics of the Helicopter. F. Ungar, 1952, p. 83.

7. Shivananda, T. P.: Pressure Measurements Near the Tip of a Hovering Model Rotor and a Preliminary Investigation of the Flow in the Rotor Wake. PhD Thesis, Georgia Institute of Technology, School of Aeronautical Engineering, Dec. 1977.

8. Jepson, D.; Moffitt, R.; Hilzinger, K.; and Bissell, J.: Analysis and Correlation of Test Data From an Advanced Technology Rotor System. NASA CR-3714, 1983.

9. Yamauchi, G. K.; and Johnson, W.: Trends of Reynolds Number Effects on Two-Dimensional Airfoil Characteristics for Helicopter Rotor Analyses. NASA TM-84363, 1983.

Table 1.– Model rotor characteristics

Scale	0.16 of full-scale S-76
Radius	1.07 m
Chord	6.3 cm
Airfoil	SC1095
Number of blades	4
Twist	–10°
Solidity	0.075

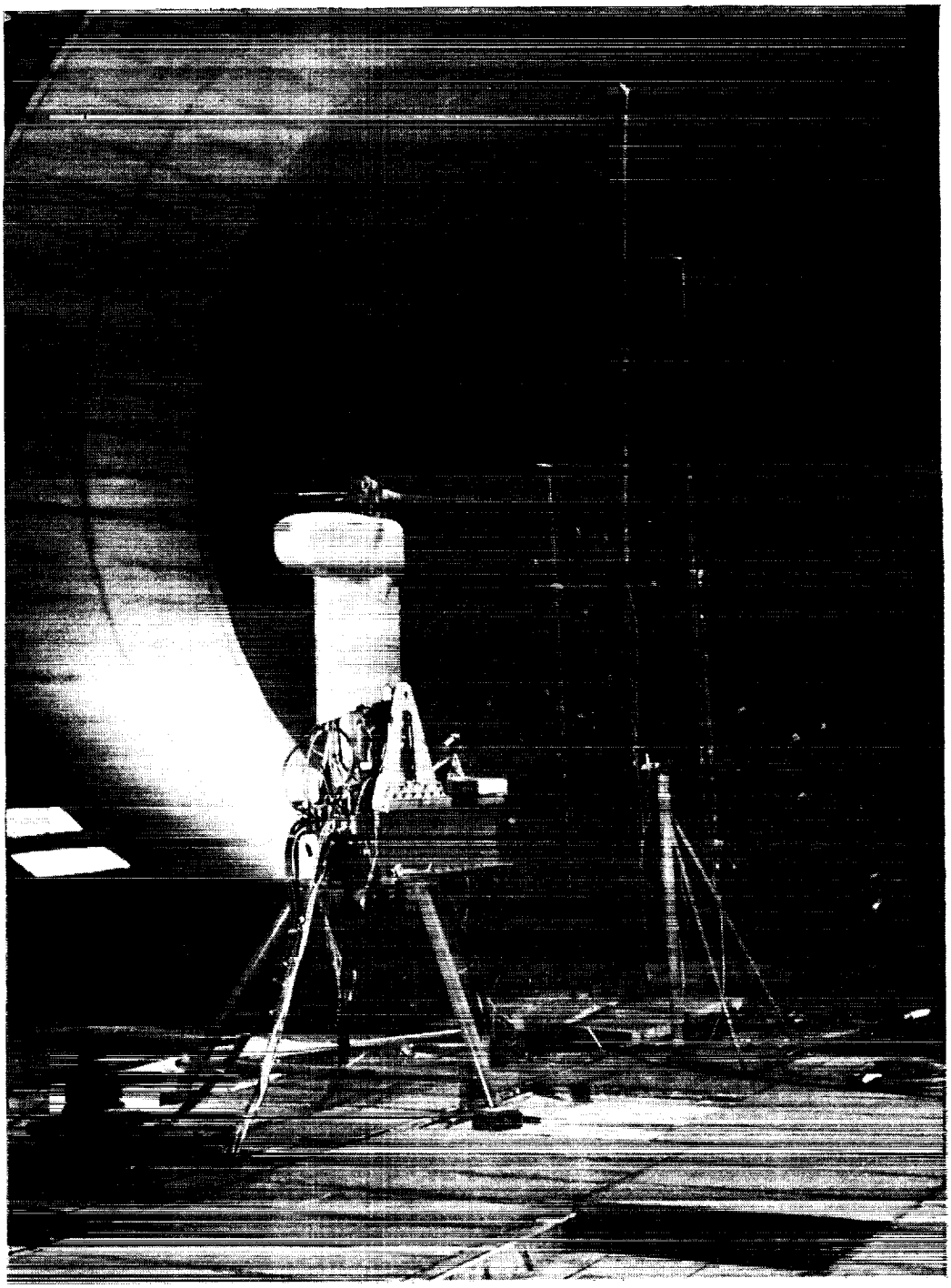

Figure 1.– Rotor Test Rig set up for the 40- by 80-Foot Wind Tunnel test.

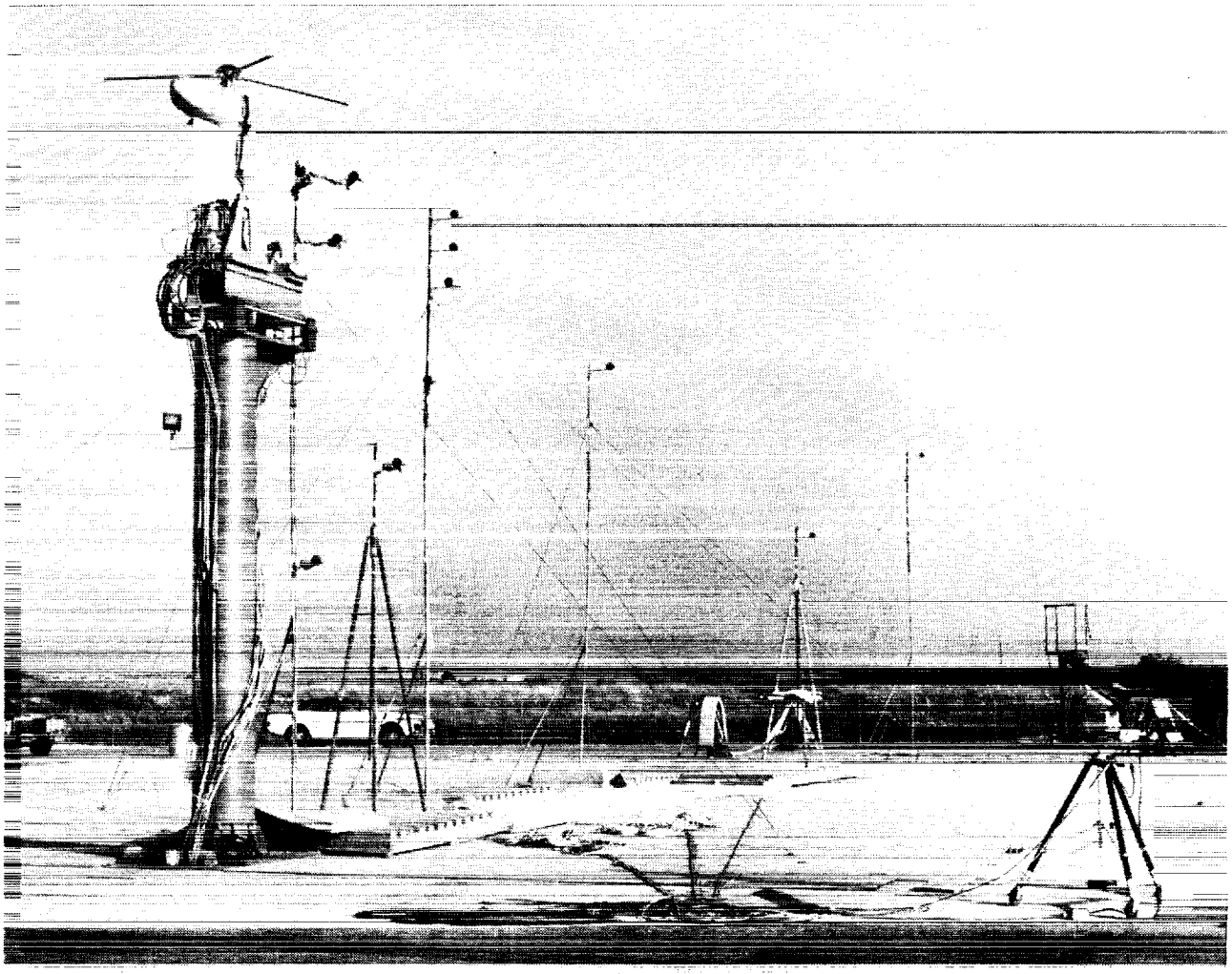

Figure 2.– Rotor Test Rig set up for the OARF I test.

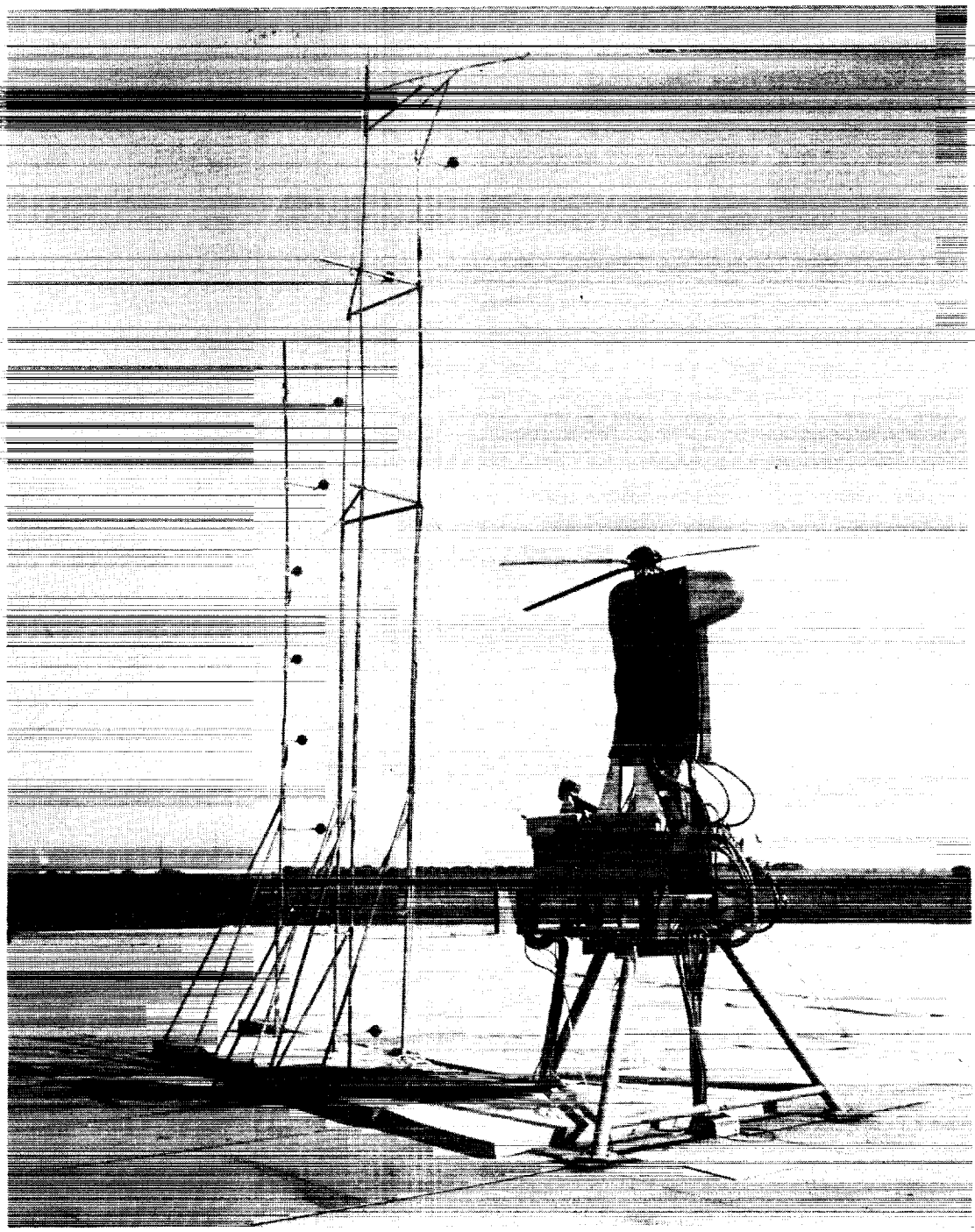

Figure 3.– Rotor Test Rig set up for the OARF II test.

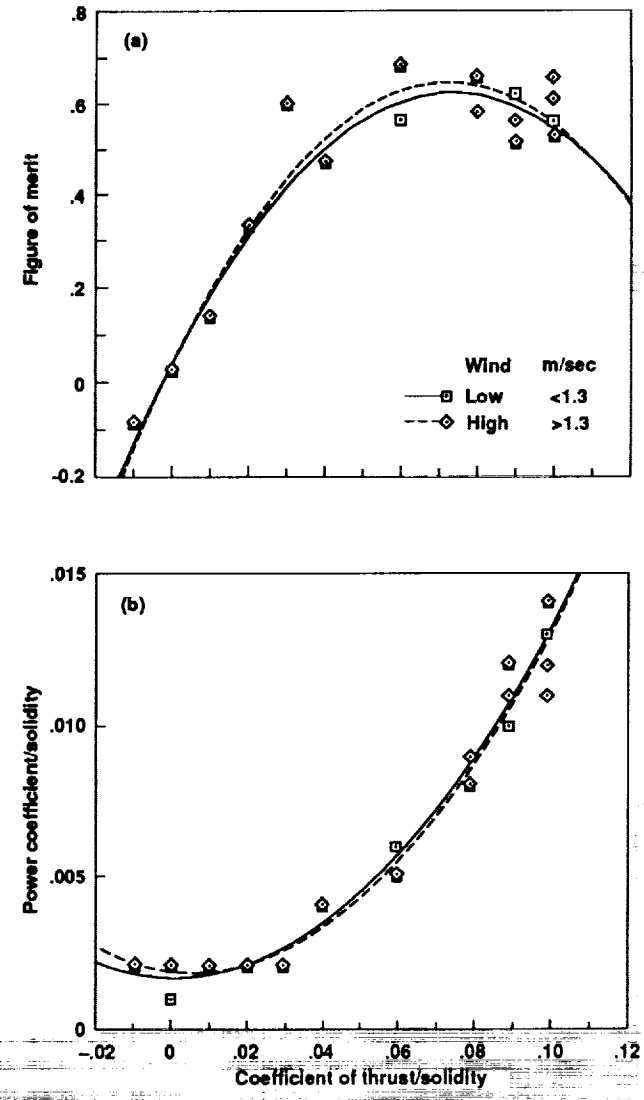

Figure 4.– Effect of wind on rotor performance—OARF I test; (a) figure of merit, (b) power coefficient/solidity.

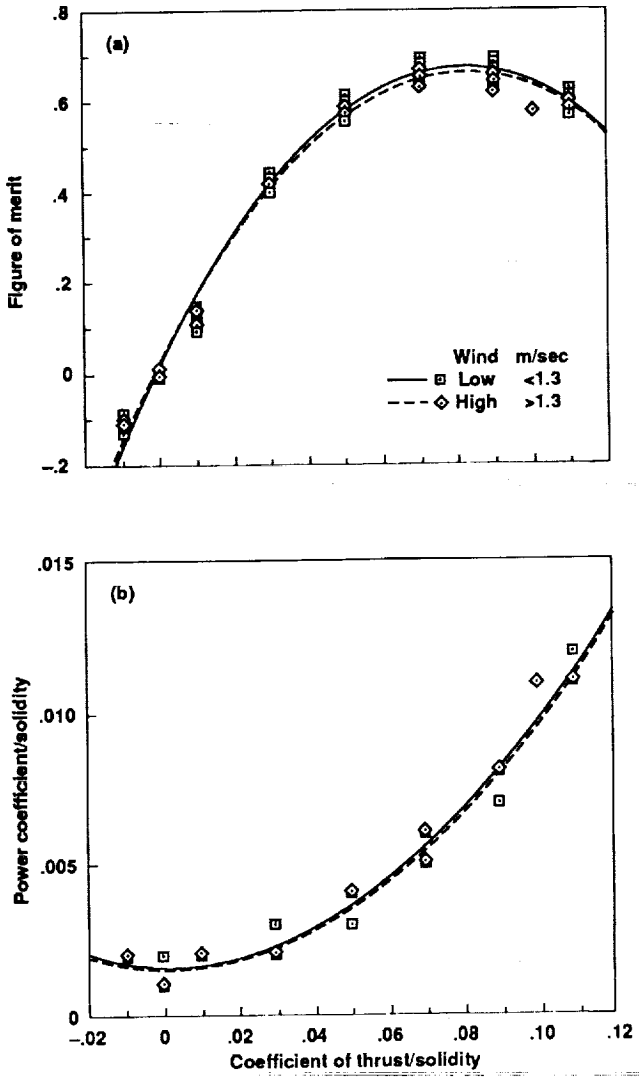

Figure 5.– Effect of wind on rotor performance—OARF II test; (a) figure of merit, (b) power coefficient/solidity.

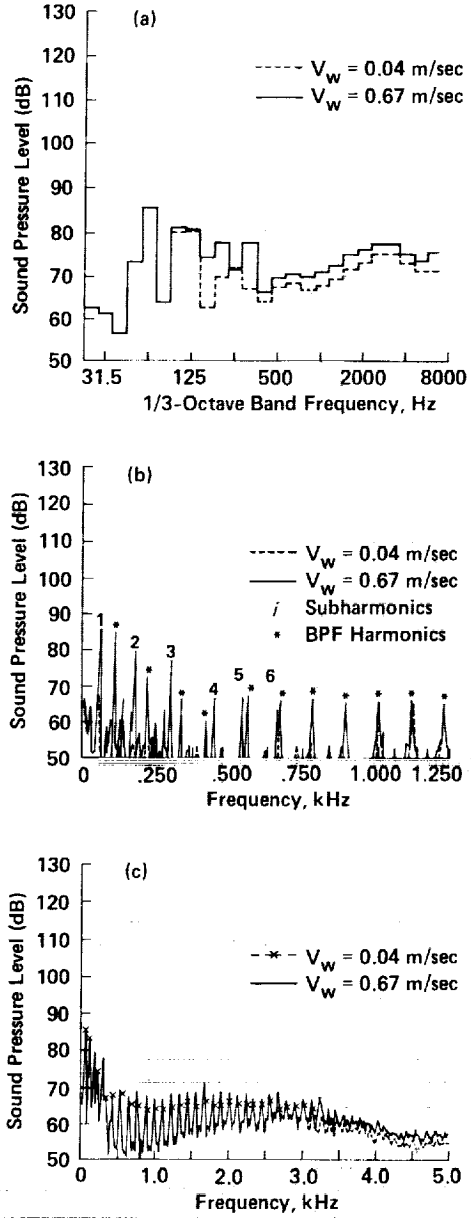

Figure 6.– Effect of wind on rotor acoustics—OARF I and II tests. Microphone is located 30° below the rotor plane at two rotor diameters from the hub. M_{tip} = 0.55, C_T/σ= 0.06. All sound pressure levels are given with respect to 2×10^{-5} N/m^2. (a) 1/3-octave-band spectrum; (b) narrow-band spectrum, 5.97-Hz bandwidth; (c) narrow-band spectrum, 23.9-Hz bandwidth.

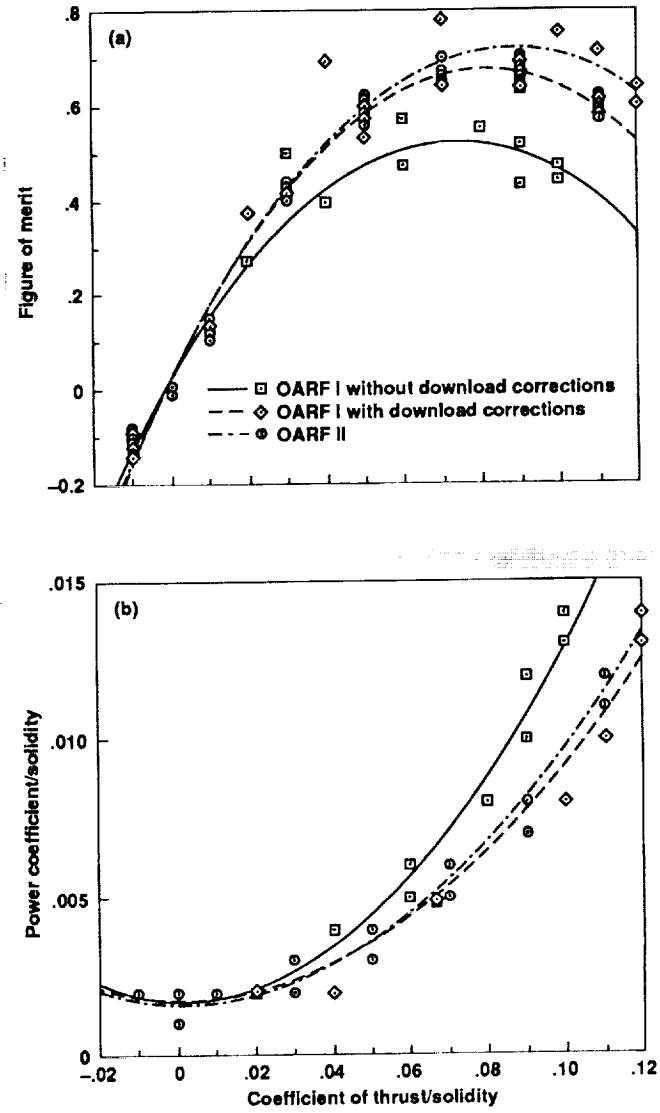

Figure 7.– Effect of test stand configuration on rotor performance; (a) figure of merit, (b) power coefficient/solidity.

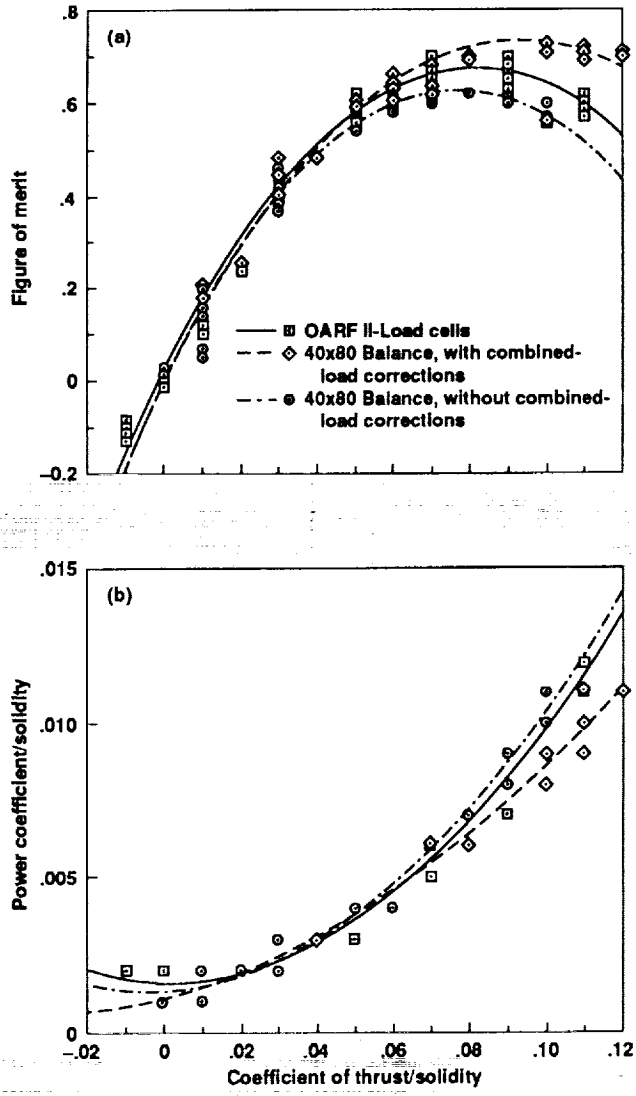

Figure 8.– Effect of test facility on rotor performance; (a) figure of merit, (b) power coefficient/solidity.

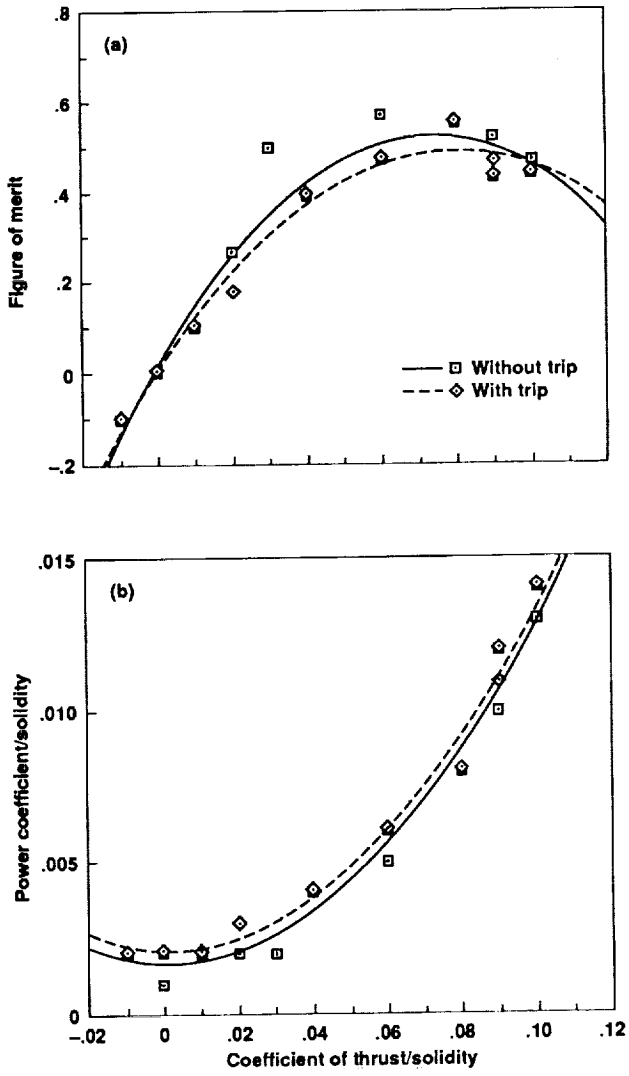

Figure 9.– Effect of boundary layer trip on rotor performance—OARF I test; (a) figure of merit, (b) power coefficient/solidity.

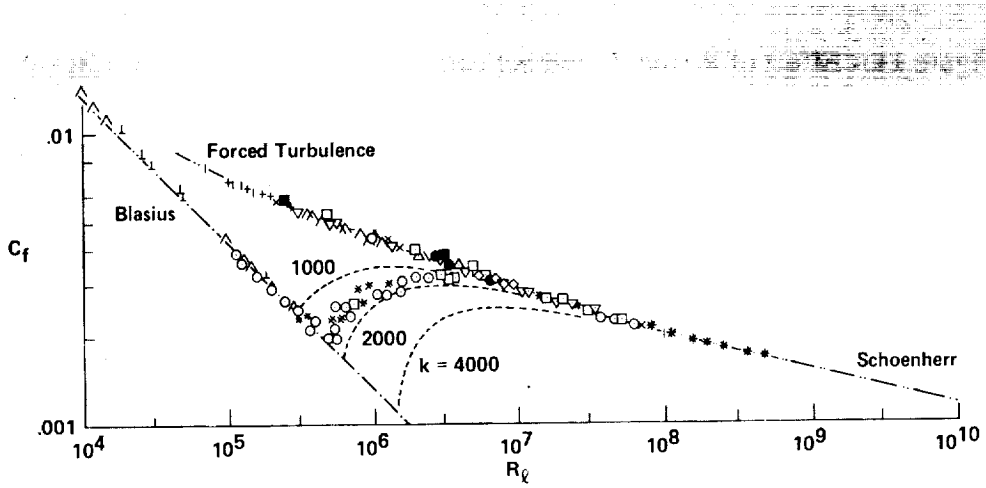

Figure 10.– Skin-friction drag coefficient of smooth and plane surfaces in incompressible flow (ref. 4).

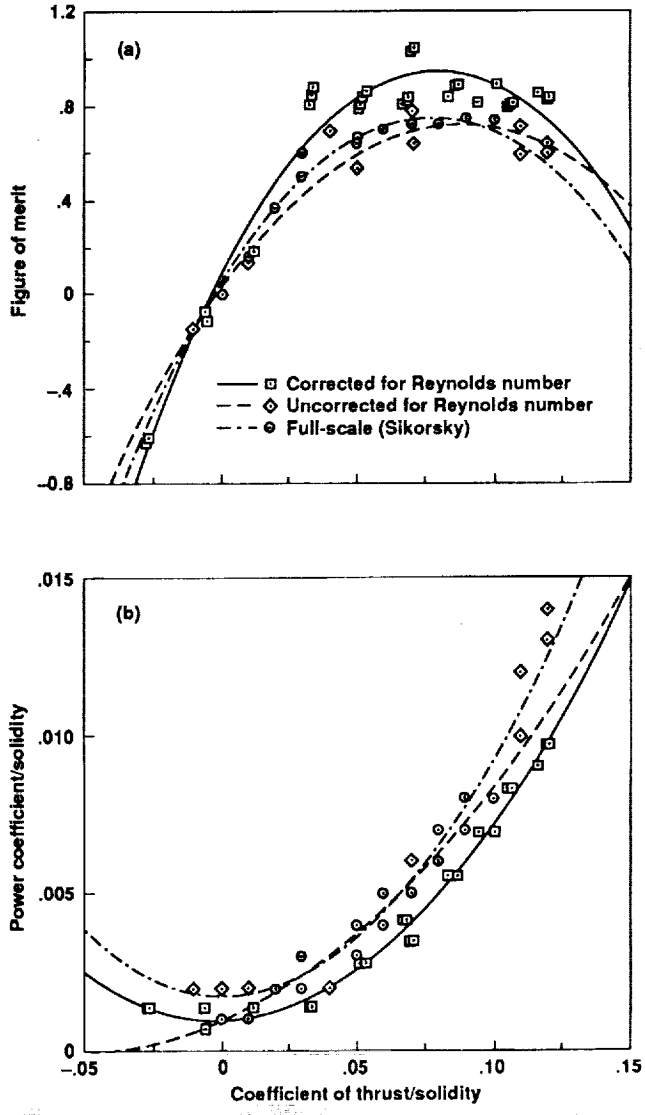

Figure 11.– Effect of Reynolds number corrections—OARF I test; (a) figure of merit, (b) power coefficient/solidity.

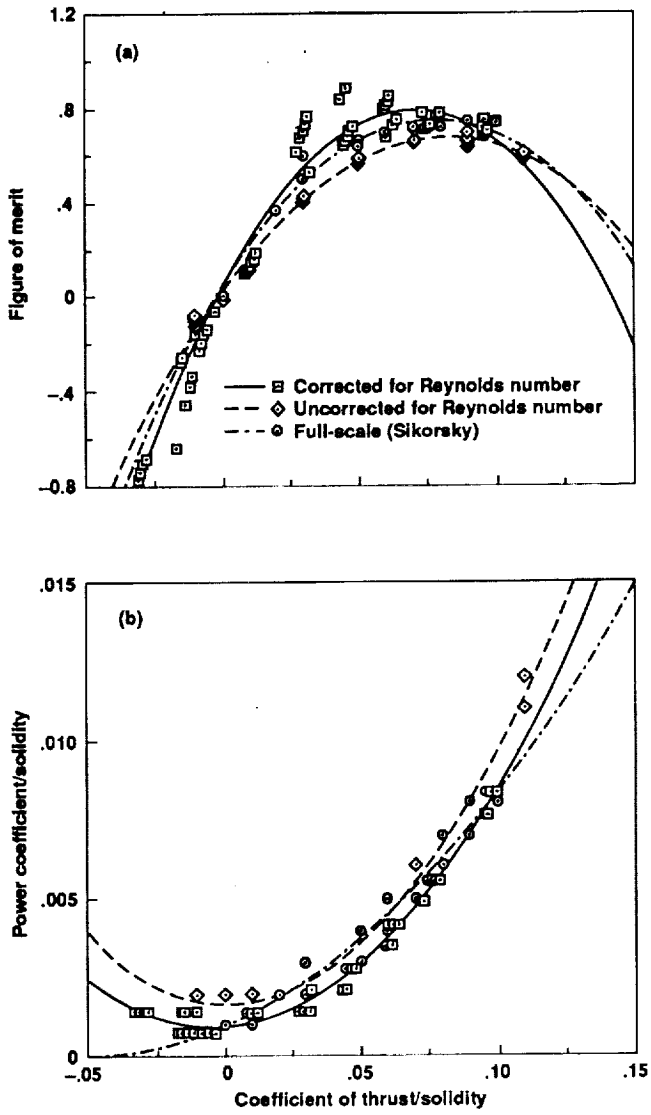

Figure 12.– Effect of Reynolds number corrections—OARF II test; (a) figure of merit, (b) power coefficient/solidity.

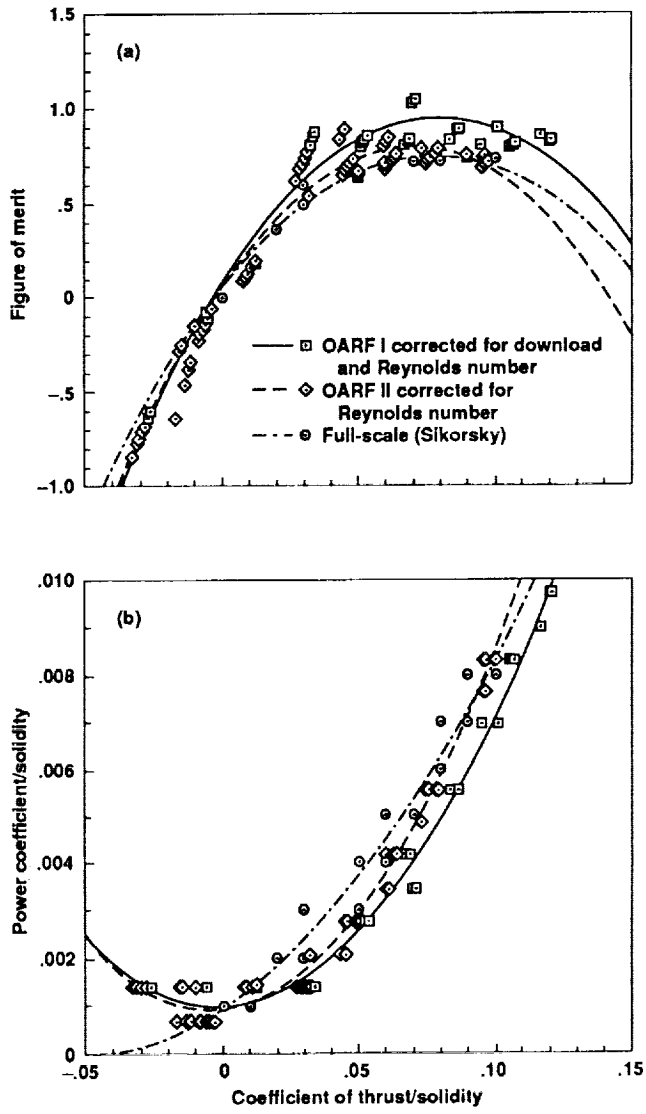

Figure 13.– Comparison of full-scale data with small-scale data corrected for Reynolds number effects; (a) figure of merit, (b) power coefficient/solidity.

NASA
National Aeronautics and Space Administration

Report Documentation Page

1. Report No.	2. Government Accession No.	3. Recipient's Catalog No.
NASA TM-102271		

4. Title and Subtitle	5. Report Date
Analysis of Small-Scale Rotor Hover Performance Data	March 1990
	6. Performing Organization Code

7. Author(s)	8. Performing Organization Report No.
Cahit Kitaplioglu	A-90046
	10. Work Unit No. 505-61-51

9. Performing Organization Name and Address	11. Contract or Grant No.
Ames Research Center Moffett Field, CA 94035-1000	
	13. Type of Report and Period Covered Technical Memorandum

12. Sponsoring Agency Name and Address	14. Sponsoring Agency Code
National Aeronautics and Space Administration Washington, DC 20546-0001	

15. Supplementary Notes

Point of Contact: Cahit Kitaplioglu, Ames Research Center, MS T042, Moffett Field, CA 94035-1000
(415) 604-6679 or FTS 464-6679

16. Abstract

Rotor hover-performance data from a 1/6-scale helicopter rotor are analyzed and the data sets compared for the effects of ambient wind, test stand configuration, differing test facilities, and scaling. The data are also compared to full-scale hover data. The data exhibited high scatter, not entirely due to ambient wind conditions. Effects of download on the test stand proved to be the most significant influence on the measured data. Small-scale data correlated reasonably well with full-scale data; the correlation did not improve with Reynolds number corrections.

17. Key Words (Suggested by Author(s))	18. Distribution Statement
Helicopter Rotor Aerodynamics	Unclassified-Unlimited Subject Category - 02

19. Security Classif. (of this report)	20. Security Classif. (of this page)	21. No. of Pages	22. Price
Unclassified	Unclassified	26	A03

NASA FORM 1626 OCT 86

For sale by the National Technical Information Service, Springfield, Virginia 22161